Enigmatic upper-plate sliver transport paused by megathrust earthquake and afterslip

T.E. Hobbs [a,*], A.V. Newman [a], M. Protti [b]

[a] *School of Earth and Atmospheric Sciences, Georgia Institute of Technology, 311 Ferst Drive, 30332, Atlanta, GA, USA*
[b] *Observatorio Vulcanológico y Sismológico de Costa Rica, 2386-3000 Heredia, Costa Rica*

A R T I C L E   I N F O

A B S T R A C T

How does deformation after an earthquake affect megathrust stresses? Five years of surface velocities following the 2012 moment magnitude 7.6 Nicoya, Costa Rica earthquake uniquely capture the lithospheric recovery. During a four-year period, seaward afterslip transitions to relocked, landward interseismic motion that matches the velocity field seen before the 2012 event. Locking reinitiates temporarily but is interrupted by late 2014 and is followed soon by a period of never-before-described, exclusively trench-parallel motion associated with a slow slip event and no resolvable megathrust locking. We present a conceptual model in which low postseismic megathrust coupling (little locking) generates partitioned slip: trench-normal motion on the megathrust during afterslip and trench-parallel motion during this never before seen transient. High coupling (strong locking) during the interseismic period drives oblique, convergent surface motions. This challenges the paradigm that megathrusts are either always partitioned or always oblique, contradicts the tectonic escape hypothesis in Central American, and introduces a new time-dependent megathrust fault behavior. Given that most subduction zones are oblique, explaining these observations is critical to characterizing stress accumulation.

Abbreviations
GNSS: Global Navigational Satellite System
PST: Postseismic Sliver Transient
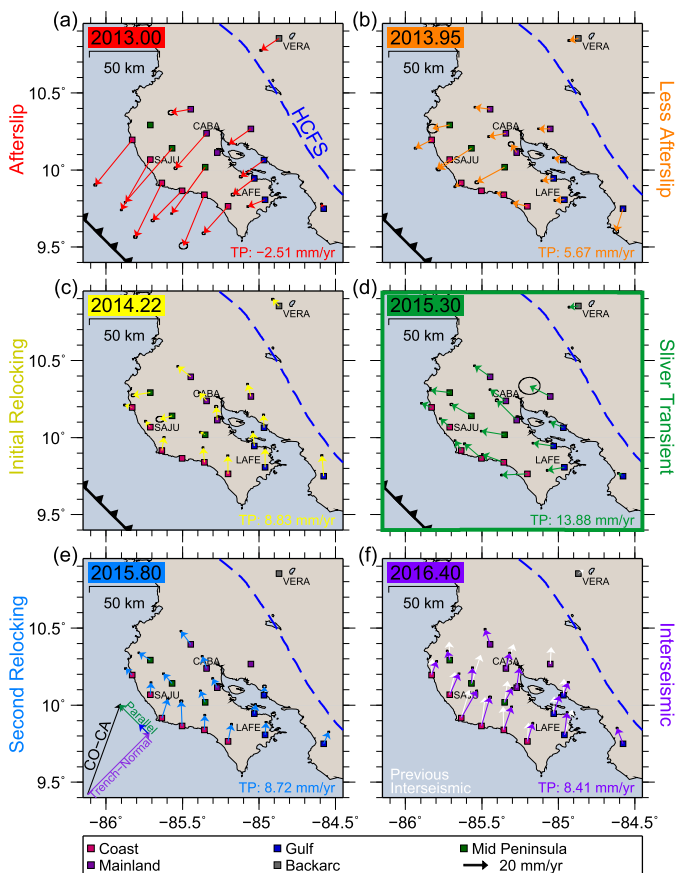SSE: Slow Slip Event

1. Introduction

The Nicoya Peninsula in Costa Rica lies on the Middle America Trench, where the Cocos plate subducts beneath the Caribbean (Fig. S1). Uncommonly, the Nicoya peninsula extends to within roughly 60 km of the trench, making it particularly attractive for land-based surface deformation measurements from directly above a seismogenic zone using Global Navigational Satellite System (GNSS) receivers. This region also has a rich earthquake history, with moment magnitude (M_w) greater than 7 events recurring approximately every 50 years (Feng et al., 2012; Protti et al., 2014). Due to the favorable geometry and short recurrence interval, GNSS and seismic networks have existed on the Nicoya Peninsula for more than two decades, recording myriad tectonic behaviors (e.g. Norabuena et al., 2004; Ghosh et al., 2008;

Outerbridge et al., 2010; Feng et al., 2012). On 5 September 2012, the most recent M_w 7.6 earthquake struck beneath Nicoya, producing up to 4 m of slip along the >100 km rupture length (Protti et al., 2014; Kyriakopoulos and Newman, 2016). This distribution of slip from this event had been forecasted prior to rupture using interseismic deformation to determine the megathrust coupling, which turned out to be an accurate method for assessing the region of future coseismic slip (Feng et al., 2012; Protti et al., 2014). Following the earthquake, several studies have detailed the postseismic response of the megathrust over several months to three years (e.g. Chaves et al., 2017; Hobbs et al., 2017; Sun et al., 2017; Voss et al., 2017), illuminating the superposition of slow slip, aftershocks, afterslip, and shallow deformation. Here, we seek to leverage recent observations to present the most complete multiyear description of megathrust relocking, as taken from directly above the seismogenic zone, to characterize the return to interseismic conditions and unique upper-plate interactions that were observed along the way.

As a result of the 25° obliquity of Cocos-Caribbean convergence at the location of the Nicoya Peninsula, the Central American Forearc translates to the northwest (LaFemina et al., 2009; Kobayashi et al., 2014) at 11 mm/yr (Feng et al., 2012). Inboard of Nicoya, margin-parallel forearc strain is accommodated by shearing across the volcanic arc, along the Haciendas-Chiripa Fault System (Fig. 1) (Feng et al., 2012; Montero et al., 2017). While sliver mo-

Fig. 1. Surface velocities, in stable Caribbean reference frame, are calculated for a one year period. Start time of that one year is shown in top left of each panel, and illustrated in Fig. 2. Network averaged trench-parallel (TP) motion indicated in bottom right corner of each panel, but not removed from GNSS velocities. Haciendas-Chiripa Fault System (HCFS) shown as dashed blue line (Kyriakopoulos and Newman, 2016; Montero et al., 2017), and Middle America Trench as black line with triangles. All available times are shown in Movie S1. Time periods are colored as follows: (a – red) strong seaward motion in January 2013, (b – orange) diminished seaward motion in December 2013, (c) slight trench-parallel motion in March 2014, (d) peak trench-parallel transient in April 2015, (e) diminished trench-parallel motion in October 2015, and (f) oblique landward motion in May 2016. Interseismic results of Feng et al. (2012) shown with white arrows on panel (f). Convergence vector and its trench-normal, trench-parallel, and sliver motion components indicated in black, purple, green, and blue arrows, respectively (DeMets et al., 2010; Feng et al., 2012) and displayed in panel (e). Coastal stations are shown in pink, mid-peninsula stations in teal, mainland stations in purple, Gulf of Nicoya stations in blue, and backarc station in grey (Table S1).

tion is assumed to be controlled by oblique subduction, the extent to which other processes affect its motion throughout phases of the seismic cycle has been undocumented until now. Such work is essential to understanding patterns of stress accumulation and release in the human-populated upper-plate portion of subduction zones.

2. Methods

2.1. Global navigation satellite system (GNSS) velocities

To understand postseismic crustal deformation, we consider GNSS observations surrounding the Nicoya peninsula. Campaign GNSS measurements were taken in 2012 (Protti et al., 2014), in 2015 and 2016 (Hobbs et al., 2017), and most recently in 2017. Temporally sparse campaign observations supplement a network of continuous GNSS stations on the Nicoya Peninsula, jointly operated by the University of South Florida and the Observatorio Vulcanológico y Sismológico de Costa Rica with technical sup-
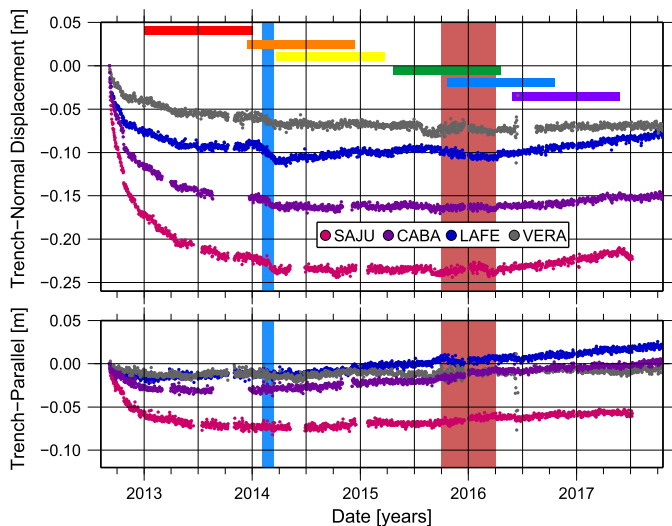
port from University NAVSTAR Consortium (http://www.unavco.org). Presented in Table S1 and Fig. S2, this study uses 23 stations for 5 years from immediately after the 2012 M_w 7.6 Nicoya earthquake to the end of January 2018. This is an extension of the time series of Hobbs et al. (2017), containing more than 1.5 more years of continuous data and one more set of campaign occupations. For the additional campaign data, we use the same precise point positioning methodology of Hobbs et al. (2017), to obtain fiducial-free daily positions (Zumberge et al., 1997) in the ITRF-2008 reference frame (Altamimi et al., 2011). For each day, velocities are obtained by taking the slope of the weighted best-fit line through the subsequent year of daily positions (Dataset S1), and converted to a stable Caribbean reference frame using the geologically-determined, globally self-consistent relative plate velocities of DeMets et al. (2010). Using shorter periods (<1 year) for velocity calculations, results in aliasing from seasonal and semi-seasonal signals, which are not removed in an effort to preserve the maximum raw tectonic signal. Velocities are decomposed into trench-parallel and trench-normal vectors using a trench orientation of 315° (Fig. S3), consistent with the Nicoya interseismic study (Feng et al., 2012).

These linear velocities tend to under-predict instantaneous velocity in the first ∼3 months after the earthquake, when displacement time series are strongly nonlinear (Fig. S3 herein, and Hobbs et al., 2017). This work, however, is focused on the several-year deformation and its orientation rather than addressing behaviors from immediately after the earthquake (see Malservisi et al., 2015; Hobbs et al., 2017; Sun et al., 2017). For this reason, short-term errors in annual velocities will minimally affect the outcome of our study. We also exclude any velocities with formal horizontal errors greater than 3 mm. This threshold is selected manually to minimize spurious velocities calculated from a small number of data points at the start or end of data intervals (Fig. S4). Formal errors are often smaller than the true uncertainty in GNSS surface velocities, without accounting for factors like scattering from tropospheric moisture. While we attempt to account for much of this by averaging over a year-long period, we also adjust by considering suites of data rather than any one particular time series from an individual station. In this way, our time series remain minimally processed to avoid filtering out region-wide, real tectonic signals that can be convolved with noise signals.

2.2. Backslip inversion for megathrust locking

To understand how the subduction interface evolves during postseismic recovery, surface velocities are used as inputs for elastic slip inversions using a fully 3D slab model (Kyriakopoulos et al., 2015). Given the same station-slab geometry, Green's functions from the inversion of Hobbs et al. (2017) are implemented into GTdef (Chen et al., 2009) using the backslip method of Savage (1983). This method is only applicable after the afterslip signal is diminished, hence we calculate backslip for times in the latter portion of our study period only.

Assuming a freely-slipping plate moves at the constant convergence rate (82.3 ± 2.2 mm/yr; DeMets et al., 2010), any degree of coupling can be modeled as relative amounts of normal slip on an otherwise stationary interface. In effect, this assigns a reference frame wherein the entire fault is sliding freely, modeled as being "stationary", and assigns backslip to portions of the fault which are retarded. This methodology therefore assumes only purely elastic, recoverable convergence of plates with no far-field deformation. Whereas trench-parallel motion is often regarded as inelastic (unrecoverable), some trench-parallel motion must be removed prior to inverting for backslip (see Norabuena et al., 2004, for further discussion). Consistent with previous studies (e.g. Norabuena et al., 2004; Wang et al., 2007), for each time period we calculate the network averaged trench-parallel velocity and remove it from each

Fig. 2. GPS displacements, in meters [m] relative to the position immediately after the 2012 M_w 7.6 Nicoya earthquake, for representative stations SAJU, CABA, LAFE, and VERA (shown in Fig. 1). Displacements are in a stable Caribbean reference frame, decomposed into trench-normal and trench-parallel components in the top and bottom panels, respectively. Vertical blue and red shaded regions denote the 2014 and 2015 slow slip events described in Voss et al. (2017). These events are most visible in the trench-normal component of motion for station SAJU, near the Gulf of Nicoya. Horizontally elongated colored rectangles at the top correspond to the representative 1-year periods over which annual velocities are calculated in Fig. 1. Time periods are colored as follows: red is strong seaward motion in 2013, orange is diminished seaward motion followed shortly by slight trench-parallel motion starting shown in yellow. Green is the peak trench-parallel motion, blue is diminished trench-parallel motion, and purple is oblique landward motion that is well developed by May 2016.

station (Table S2). This allows us to image the spatial progression of the relocking between the Cocos and Caribbean Plates, assuming that the majority of trench-parallel motion is related to unrecoverable sliver motion rather than convergence. To demonstrate, however, that our results are robust to this choice to remove average trench-parallel motion, supplementary Fig. S5 shows the results for the time period of maximum trench-parallel motion (green) calculated by removing the previously documented 11 mm/yr sliver motion (Feng et al., 2012), and when the 2015 SSE signal (Voss et al., 2017) is removed. All results show the same result under the central peninsula and have similar misfits, confirming that, within reasonable limits, the findings here are insensitive to varying the amount of trench-parallel slip removed prior to inversion.

In an underdetermined inversion, damping is applied and a preferred solution is found by minimizing the model fit and solution roughness (Fig. S6). Model predictions for surface velocities are compared against observed velocities to ensure the model produces realistic ground motions (Fig. S7), and from the resolution matrix we determine the area of resolvability (Fig. S8). Though our model cannot resolve locking up to the trench or at the edges of the model space, the match between modeled surface velocities and those observed suggests the results near the peninsula are reasonable.

3. Results

3.1. Relocking period features unexpected trench parallel motions

Annual GNSS surface velocities show intriguing features over the five year postseismic period (Movie S1, Fig. 1), which can be divided into six representative start dates: dominant afterslip (2013.00 – red), diminished afterslip (2013.95 – orange), initial relocking with minor trench-parallel motion (2014.22 – yellow), maximum trench-parallel motion (2015.30 – green), second relock-

ing (2015.80 – blue), and return to interseismic motions (2016.40 – purple). Note that we chose these stages to best represent the most important features and phases during the 5 year postseismic period, and thus they need not be evenly spaced. We refer to 'afterslip' as the time in which surface velocities are seaward following the earthquake, 'interseismic' as surface velocities that are landward and mimic the previous interseismic period, and 'relocking' as the time between afterslip and interseismic. Fig. 2 shows the raw displacement timeseries in their trench-normal and trench-parallel components for 4 representative continuous stations shown labeled Fig. 1. Visible in this figure are two slow slip events that occurred beneath the Gulf of Nicoya in 2014 and 2015 (Voss et al., 2017). Surface velocities are also decomposed into azimuth, trench-normal, and trench-parallel time series (Fig. S3). In both Figs. 1, 2 and S3 we see a progression from trench-normal afterslip that, between late-2013 (Fig. 1b) and early-2014 (Fig. 1c), decays and rotates towards purely trench-parallel motion (Fig. 1d). This is followed in late-2015 by continued rotation towards oblique landward convergence (Fig. 1e), with coastal stations then inland stations returning to near-interseismic velocities seen prior to the 2012 earthquake (Fig. 1f). The relocking period, it seems, is interrupted by a period of purely trench-parallel velocity across the entire forearc sliver. Hereon, this period will be referred to as the Postseismic Sliver Transient (PST).

3.2. Relocking in two phases

Fig. 3 shows megathrust locking (coupling) during the latter 4 stages described in Fig. 1: relocking initiation (yellow), sliver transport (green), second relocking (blue), and interseismic (purple). Note that we select only time periods for which we expect little or no afterslip (Fig. 1c-f, showing no seaward motion). Before inverting the velocity field, the average trench-parallel velocity at that time was removed, representing an assumed northwestward rigid block translation (see Section 2.2 for discussion). We find that interface locking initiates contemporaneously with decaying afterslip (Fig. 3a), but then nearly disappears during the maximum PST (Fig. 3b). Ephemeral relocking, in which locking initiates but then diminishes, has not been documented previously.
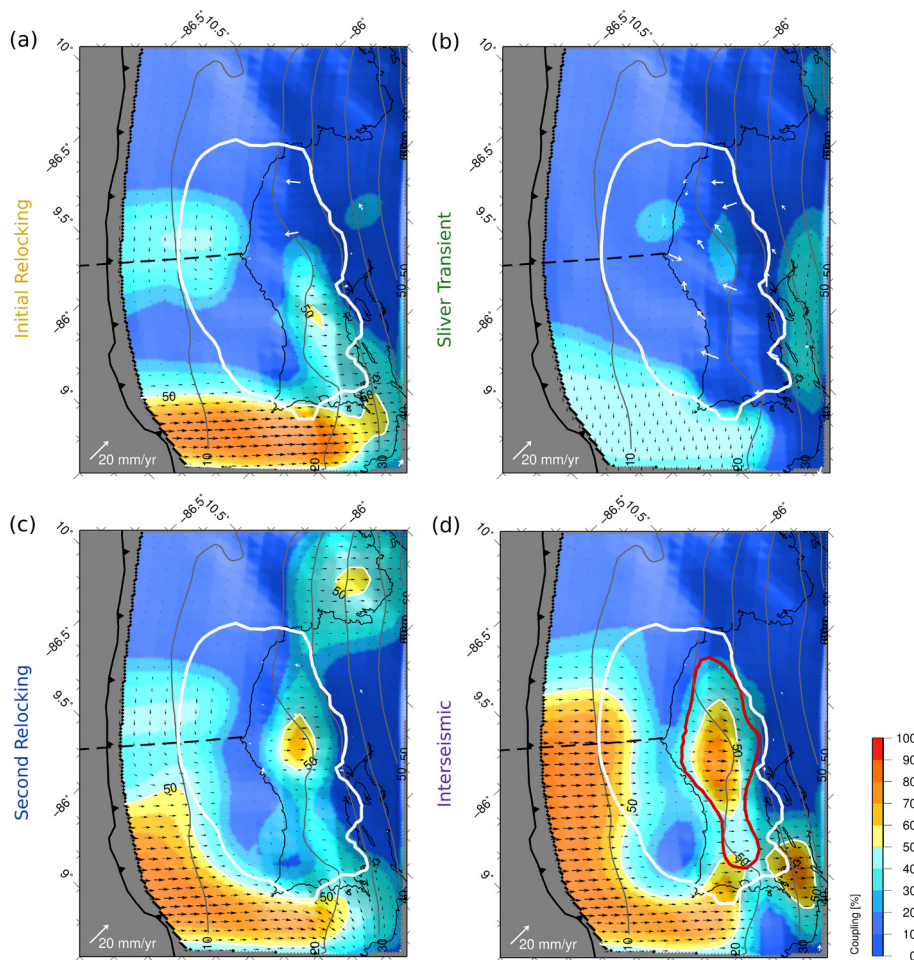
3.3. The Nicoya earthquake patch

After the PST, locking again increases and forms a highly locked patch under the center of the peninsula. This patch is collocated with the area of highest locking in the previous interseismic period (Feng et al., 2012; Kyriakopoulos and Newman, 2016) and the maximum coseismic slip (Protti et al., 2014; Kyriakopoulos and Newman, 2016). It is also an area that was devoid of afterslip and aftershocks (Hobbs et al., 2017). This suggests it may be a permanent velocity-weakening asperity through multiple earthquake cycles: focusing stress accumulation during the interseismic and rupturing energetically during large coseismic events roughly every 50 years (Feng et al., 2012).

4. Discussion

4.1. Relocking timeline

Initiation of relocking on the rupture patch 3 years after the mainshock is slower than expected (Remy et al., 2016; Bedford et al., 2016), and the full interseismic velocity field (16.4 ± 4.9 cm/yr at 11.1 ± 16.0°) is only attained by mid-2016. Subtracting 4 years postseismic from the interseismic energy budget accounts for up to 0.33 m of potential slip, based on convergence at 82 mm/yr (DeMets et al., 2010) and depending on the amount of partial coupling attained during the relocking period. This suggests that

Fig. 3. Result of backslip inversions during (a) PST initiation, (b) maximum PST, (c) post PST, and (d) the end of the study period, including red contour showing the area of greater than 1 m coseismic slip (Kyriakopoulos and Newman, 2016). Proportion of maximum total coupling is colored and contoured, relative to 83 mm/yr convergence (DeMets et al., 2010), with black vectors indicating the direction of hanging wall motion. Average trench-parallel velocities for each time period are removed prior to inversions, as discussed in method, but locking is allowed in either trench-parallel direction and normal faulting (backslip). White vectors show residual horizontal velocities between model and observations (Fig. S6), with scale in bottom left of each panel showing 20 mm/yr of residual velocity. Interface geometry shown by grey contours (Kyriakopoulos et al., 2015). Middle America Trench shown as solid line with triangles, and area of recoverability indicated by the thick white line (Fig. S7). Model misfit evaluations can be found in Fig. S5.

accurately constraining recovery timescales is critical to estimating accumulated stress, rather than simply assuming it accumulates over the full inter-event time.

4.2. Novel observation of variable trench-parallel velocity

Afterslip and relocking are expected in the current paradigm of postseismic recovery (Wang et al., 2012), however the interruption for exclusively trench-parallel motion observed between 2013.95 and 2015.80, was not. Sliver transport rates are generally considered to be constant (e.g. Jarrard, 1986; McCaffrey, 1992, 2002; Lundgren et al., 1999; Bevis and Martel, 2001; Norabuena et al., 2004; LaFemina et al., 2009; Feng et al., 2012), but we observe substantial variability across the PST (Fig. S3). Averaged across the forearc and over the entire PST, surface velocity is 9.2 ± 4.5 mm/yr and -0.1 ± 7.2 mm/yr in the trench-parallel and trench-normal directions, respectively. The average azimuth of velocities during the PST is $317 \pm 39°$, indistinguishable from the trench azimuth of $315°$ (Fig. S3). In other words, we know that there is an unexpected period in which the motion of the sliver is purely trench-parallel. This trench-parallel velocity is similar or slightly larger than the 11 mm/yr interseismic value (Feng et al., 2012), and 1.7-2.7 times larger than earlier sliver transport estimates for this region (McCaffrey, 2002; Norabuena et al., 2004;

LaFemina et al., 2009). During the maximum PST (2015.30), trench-parallel velocity is 13.3 ± 5.7 mm/yr. Conversely, it reaches its minimum in the early portion of the postseismic recovery period, where appreciable trench parallel motion is absent. During this time, we even find slightly negative trench-parallel velocities, with the largest signals occurring at coastal and Mid-Peninsula sites (Fig. S3). This has important ramifications for estimates of long-term sliver motion, which are often calculated assuming a constant velocity. Trench-normal interseismic strain is modeled as a sum of linear convergence and episodic SSE's. This finding suggests that trench-parallel velocities require similar treatment, especially as relative fault strength changes through the seismic cycle. Our result also raises the question: What is causing this variable sliver velocity? To answer this, we consider conditions in and around the Nicoya megathrust and the portion of the Central American Forearc Sliver that overlies it.

4.2.1. Relationship to megathrust slow slip events

Two Slow Slip Events (SSEs) occurred during the postseismic period, with one in early 2014 lasting from early February to mid-March (2014.09-2014.20), and a longer event from late 2015 to early 2016 (2015.75-2016.25) (Voss et al., 2017). Slip from these events was located primarily in the Gulf of Nicoya, with a small component offshore near the center of the Peninsula and another

patch beneath the mainland just south of the Gulf of Nicoya (Voss et al., 2017). The 2014 SSE is coincident with the onset of the PST and the first peak in trench-parallel motion, while the longer 2015 SSE initiates at the termination of the PST event (Fig. S3). Removing the 2015 SSE velocities prior to inversion (Fig. S5) does not significantly affect results. Bounded temporally by SSEs, a relationship between the sliver transient and other transient fault behavior of the megathrust below is possible. Although we cannot say for certain which came first, initiation of a SSE may be the source of the apparent disruption of the initial locking phase. Further studies should focus on modeling to better determine the possible link between SSE, megathrust relocking, and trench-parallel movement.

4.2.2. Relationship to the Haciendas-Chiripa Arc Fault
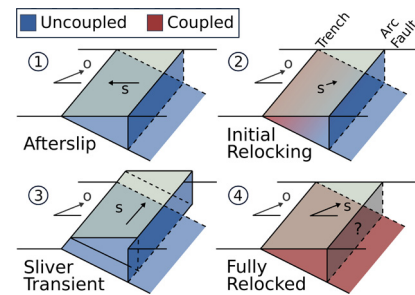
Following a large megathrust event, the upper plate is under extension (e.g. Sun et al., 2014), which equates to unclamping of the arc fault and subsequent triggering of seismicity or volcanism (e.g. Lupi and Miller, 2014; Lupi et al., 2014; Spagnotto et al., 2015). Both our study and prior observations suggest differential motion of the stable Caribbean plate relative to the Central American Forearc is accommodated through the volcanic arc (Lundgren et al., 1999; Norabuena et al., 2004; Feng et al., 2012; Montero et al., 2017). The Haciendas-Chiripa Fault (Fig. 1) has been mapped through much of the arc inboard of the Nicoya Peninsula, serving as the main transcurrent fault in this oblique system. Since the PST is defined by unexpected trench-parallel motion, this major strike slip fault system is likely involved and may play a critical role in accumulating the driving stress.

To investigate the role of the arc fault in the observed sliver transient, we searched for changes in regional (http://www.ovsicori.una.ac.cr) and arc-related seismicity (Chaves et al., 2017; Montero et al., 2017), as well as in eruptive activity (http://volcano.si.edu) concurrent with the PST. Given current limited datasets (Figs. S9-11), there is no discernable deviation between the pre-PST, PST, and post-PST periods. However, this may reflect insufficient observations rather than a true paucity of activity on the HCFS during this sliver transient. Further to the south a regional seismic network on the Turrialba-Irazú complex recorded an earthquake swarm immediately following the 2012 Nicoya earthquake, suggesting a dynamic triggering link between the megathrust and arc-related faults in Costa Rica (Lupi et al., 2014). Furthermore, previous damaging earthquakes have occurred on the steeply dipping, arc-bounding HCFS (Lewis et al., 2017). This suggests that the arc fault is indeed capable of accumulating margin-parallel stress from oblique subduction and subsequently behaving in a stick-slip manner. Therefore, a denser local seismic network, additional back arc GPS stations, and catalog relocation may be crucial to assess the possibility of heightened arc fault-related seismicity during the PST and to fully understand this novel phenomenon.

4.2.3. Preliminary conceptual model of PST

To understand how these observations may be relevant to other subduction zones it is important to ask: What is driving the postseismic sliver transient? Oblique convergence is shown to result in oblique surface velocities in the upper-plate when overall coupling on the megathrust interface is relatively strong, and partitioned slip when coupling is relatively weak (Jarrard, 1986). Thus, different subduction zones have different behavior. However, our observations suggest this is not the full story.

For the interseismic periods (before 2012 and after 2016), surface velocities are oblique landward and the megathrust is well-coupled (Feng et al., 2012). The presence of afterslip proves that coupling was low on the megathrust, because differential motion was occurring on it (Hobbs et al., 2017), and also suggests that coupling on the Haciendas-Chiripas arc fault system is likely to

Fig. 4. Conceptual model of forearc motions observed herein, delineated along the megathrust interface (inclined plane) and arc-bounding fault (vertical). This model is generalized beyond the study area, but surface velocities are consistent with those observed in Figs. 1 and S7. The incoming oceanic plate, marked by vector "o", maintains oblique convergence. Representative surface velocities shown as vector "s". Blue faults are poorly coupled or unclamped, and red indicates that the fault is relatively well-coupled or strong. During (1) afterslip, the forearc moves seaward in a trench-normal direction, sliding along a weakly-coupled megathrust and unclamping the arc fault. We do not know how long the arc fault might remain unclamped, but suspect it could persist through the PST. The afterslip is driven by stored elastic stress and coseismic stress changes. As (2) relocking initiates, coupling increases in the shallow megathrust and seaward velocities are diminished or gently reversed. This is indicated by a quasi-coupled megathrust. (3) During the PST, coupling is low on the megathrust and arc fault but stored compressional stresses were already released by afterslip. Partitioning of slip during the PST thus results in purely trench-parallel sliver motion. (4) Relocking reinitiates, and eventually the megathrust is highly coupled. Slip is no longer partitioned, and stress accumulates in the direction of convergence, regardless of the state of the arc-bounding fault.

have weakened due to relative elastic extension in the upper-plate (Lupi and Miller, 2014). In an oblique convergent margin we expect this to promote dextral slip across the arc fault, consistent with observed short-lived, trench-parallel forearc motion we see during the PST. Concurrently, we have shown herein that megathrust coupling at that time was very low. Therefore, during afterslip and the PST, when we see partitioning of surface velocities between trench-normal and trench-parallel, respectively, the megathrust fault coupling is low and the arc fault is likely unclamped. We propose that partitioning or oblique motion is indeed impacted by megathrust conditions, but that variations in interface strength can drive differing behavior at a single subduction zone. This is suggested by the association between megathrust variability through the postseismic period (Fig. 4) that corresponds to sliver motion when coupling is weak, and oblique surface motions when coupling is strong.

Interseismic velocities were assumed to be constant, until months-long, episodic slow slip events (SSE) were first observed in Cascadia (Dragert et al., 2001). We now well understand that deformation rates change within the seemingly stable megathrust interseismic period (Meltzner et al., 2015). The results presented herein tell a similar story, for trench-parallel velocities of the sliver. Could it be that the variable sliver velocity we observe here is not a one-off, but rather is the first observation of a phenomenon occurring at other subduction zones as well? To validate or refine this preliminary conceptual model, we must start looking for temporary instances of partitioned slip, particularly transient sliver motions, that can be then be tied to changes in megathrust conditions.

4.3. Tectonic drivers

Slivers, which are well-developed on at least half of all subduction zones, migrate along the plate margin causing potentially thousands of kilometers of translation over tens of millions of years (Jarrard, 1986). According to previous studies, the motion of a forearc sliver occurs either through oblique subduction, on strong megathrusts, or through partitioning of slip into trench-normal megathrust events and trench-parallel motions across transverse

arc faults, when the megathrust is relatively weak (Jarrard, 1986). The northwest motion of the Nicoya sliver, however, has alternatively been interpreted as the result of subduction of the Cocos Ridge, which drives the Caribbean plate outward (LaFemina et al., 2009; Kobayashi et al., 2014). This model of forearc translation, invoking 'tectonic escape' from the indenting Cocos Ridge (LaFemina et al., 2009; Kobayashi et al., 2014), would result in constant forcing from the southeast at all times in Nicoya's seismic cycle. However, the time-variable nature of sliver transport during the 5-yr postseismic period, which varies from null to >10 mm/yr (Fig. S3), is likely not compatible with any model invoking a constant lateral forcing such as from an indenting ridge. This finding therefore suggests that the tectonic escape model may not be sufficient for modeling of Central American tectonics. Additional modeling will be needed to fully examine potential driving forces for this novel phenomenon.

5. Conclusions

Examining 5 years of postseismic surface deformation directly over the source region of the September 2012 M_w 7.6 Nicoya earthquake has uniquely provided an opportunity to image the evolution of megathrust relocking as it enters into the early interseismic portion of the seismic cycle. We identify that trench-normal afterslip clearly decays within two years (by late-2014), and an initial relocking signal is interrupted synchronously with a slow slip event on the megathrust. Within a few months, a novel period of purely trench-parallel motion is observed across the entire forearc region, and can be modeled to show that the feature occurs when little trench-normal coupling is occurring on the megathrust interface. Almost 4 years following the earthquake (by mid-2016), interseismic velocities return to oblique pre-2012 levels across the Peninsula, accompanied by substantial locking again below the central portion of the megathrust.

The relationship between slip partitioning and megathrust coupling is unlikely coincidental, with strongly partitioned motion during periods of low megathrust coupling and oblique motion when locking is high. These findings are inconsistent with the tectonic escape model of Central American tectonics, by documenting that sliver transport does not occur at a constant rate and may change depending on the coupling along the megathrust interface. This variable sliver transport rate is an important finding for understanding long term sliver translation. Although we present a preliminary conceptual framework to explain these observations, future work should seek a cause for the interruption of relocking processes associated with the decrease in coupling and start of the postseismic sliver transient. Explaining these observations will be crucial in developing a complete understanding of the megathrust earthquake cycle and associated time-dependent hazards.

Acknowledgements

Appendix A. Supplementary material

Supplementary material related to this article can be found online at https://doi.org/10.1016/j.epsl.2019.05.016.

References

Altamimi, Z., Collilieux, X., Métivier, L., 2011. ITRF2008: an improved solution of the international terrestrial reference frame. J. Geod. 85 (8), 457–473.

Bedford, J., Moreno, M., Li, S., Oncken, O., Carlos Baez, J., Bevis, M., Heidbach, O., Lange, D., 2016. Separating rapid relocking, afterslip, and viscoelastic relaxation: an application of the postseismic straightening method to the Maule 2010 cGPS. J. Geophys. Res., Solid Earth 121 (10), 7618–7638. https://doi.org/10.1002/2016JB013093.

Bevis, M., Martel, S.J., 2001. Oblique plate convergence and interseismic strain accumulation. Geochem. Geophys. Geosyst. 2 (8).

Chaves, E.J., Duboeuf, L., Schwartz, S.Y., Lay, T., Kintner, J., 2017. Aftershocks of the 2012 M_w 7.6 Nicoya, Costa Rica, earthquake and mechanics of the plate interface. Bull. Seismol. Soc. Am. 107 (3), 1227–1239.

Chen, T., Newman, A.V., Feng, L., Fritz, H.M., 2009. Slip distribution from the 1 April 2007 Solomon Islands earthquake: a unique image of near-trench rupture. Geophys. Res. Lett. 36 (16).

DeMets, C., Gordon, R.G., Argus, D.F., 2010. Geologically current plate motions. Geophys. J. Int. 181 (1), 1–80.

Dragert, H., Wang, K., James, T.S., 2001. A silent slip event on the deeper Cascadia subduction interface. Science 292 (5521), 1525–1528.

Feng, L., Newman, A.V., Protti, M., Gonzalez, V., Jiang, Y., Dixon, T.H., 2012. Active deformation near the Nicoya Peninsula, northwestern Costa Rica, between 1996 and 2010: interseismic megathrust coupling. J. Geophys. Res., Solid Earth 117 (B6).

Ghosh, A., Newman, A.V., Thomas, A.M., Farmer, G.T., 2008. Interface locking along the subduction megathrust from b-value mapping near Nicoya Peninsula, Costa Rica. Geophys. Res. Lett. 35 (1).

Hobbs, T.E., Kyriakopoulos, C., Newman, A.V., Protti, M., Yao, D., 2017. Large and primarily updip afterslip following the 2012 Mw 7.6 Nicoya, Costa Rica earthquake. J. Geophys. Res., Solid Earth 122 (7), 5712–5728.

Jarrard, R.D., 1986. Terrane motion by strike-slip faulting of forearc slivers. Geology 14 (9), 780–783.

Kobayashi, D., LaFemina, P., Geirsson, H., Chichaco, E., Abrego, A.A., Mora, H., Camacho, E., 2014. Kinematics of the western Caribbean: collision of the Cocos Ridge and upper plate deformation. Geochem. Geophys. Geosyst. 15 (5), 1671–1683.

Kyriakopoulos, C., Newman, A.V., Thomas, A.M., Moore-Driskell, M., Farmer, G.T., 2015. A new seismically constrained subduction interface model for Central America. J. Geophys. Res., Solid Earth 120 (8), 5535–5548.

Kyriakopoulos, C., Newman, A.V., 2016. Structural asperity focusing locking and earthquake slip along the Nicoya megathrust, Costa Rica. J. Geophys. Res., Solid Earth 121 (7), 5461–5476.

LaFemina, P., Dixon, T.H., Govers, R., Norabuena, E., Turner, H., Saballos, A., Mattioli, G., Protti, M., Strauch, W., 2009. Fore-arc motion and Cocos Ridge collision in Central America. Geochem. Geophys. Geosyst. 10 (5).

Lewis, J.C., Montero Pohly, W.K., Araya, M.C., 2017. Crustal seismicity and geomorphic observations of the Chiripa-Haciendas Fault system: the Guanacaste volcanic arc sliver of western Costa Rica. In: AGU Fall Meeting Abstracts. December.

Lundgren, P., Protti, M., Donnellan, A., Heflin, M., Hernandez, E., Jefferson, D., 1999. Seismic cycle and plate margin deformation in Costa Rica: GPS observations from 1994 to 1997. J. Geophys. Res., Solid Earth 104 (B12), 28915–28926.

Lupi, M., Fuchs, F., Pacheco, J.F., 2014. Fault reactivation due to the M7. 6 Nicoya earthquake at the Turrialba-Irazú volcanic complex, Costa Rica: effects of dynamic stress triggering. Geophys. Res. Lett. 41 (12), 4142–4148.

Lupi, M., Miller, S.A., 2014. Short-lived tectonic switch mechanism for long-term pulses of volcanic activity after mega-thrust earthquakes. Solid Earth 5 (1), 13.

Malservisi, R., Schwartz, S.Y., Voss, N., Protti, M., Gonzalez, V., Dixon, T.H., Jiang, Y., Newman, A.V., Richardson, J., Walter, J.I., Voyenko, D., 2015. Multiscale postseismic behavior on a megathrust: the 2012 Nicoya earthquake, Costa Rica. Geochem. Geophys. Geosyst. 16 (6), 1848–1864.

McCaffrey, R., 1992. Oblique plate convergence, slip vectors, and forearc deformation. J. Geophys. Res., Solid Earth 97 (B6), 8905–8915.

McCaffrey, R., 2002. Crustal block rotations and plate coupling. In: Plate Boundary Zones, pp. 101–122.

Meltzner, A.J., Sieh, K., Chiang, H.W., Wu, C.C., Tsang, L.L., Shen, C.C., Hill, E.M., Suwargadi, B.W., Natawidjaja, D.H., Philibosian, B., Briggs, R.W., 2015. Time-varying interseismic strain rates and similar seismic ruptures on the Nias–Simeulue patch of the Sunda megathrust. Quat. Sci. Rev. 122, 258–281.

Montero, W., Lewis, J.C., Araya, M.C., 2017. The Guanacaste Volcanic Arc Sliver of Northwestern Costa Rica. Sci. Rep. 7.

Norabuena, E., Dixon, T.H., Schwartz, S., DeShon, H., Newman, A., Protti, M., Gonzalez, V., Dorman, L., Flueh, E.R., Lundgren, P., Pollitz, F., 2004. Geodetic and seismic constraints on some seismogenic zone processes in Costa Rica. J. Geophys. Res., Solid Earth 109 (B11).

Outerbridge, K.C., Dixon, T.H., Schwartz, S.Y., Walter, J.I., Protti, M., Gonzalez, V., Biggs, J., Thorwart, M., Rabbel, W., 2010. A tremor and slip event on the Cocos-Caribbean subduction zone as measured by a global positioning system (GPS) and seismic network on the Nicoya Peninsula, Costa Rica. J. Geophys. Res., Solid Earth 115 (B10).

Protti, M., González, V., Newman, A.V., Dixon, T.H., Schwartz, S.Y., Marshall, J.S., Feng, L., Walter, J.I., Malservisi, R., Owen, S.E., 2014. Nicoya earthquake rupture anticipated by geodetic measurement of the locked plate interface. Nat. Geosci. 7 (2), 117.

Remy, D., Perfettini, H., Cotte, N., Avouac, J.P., Chlieh, M., Bondoux, F., Sladen, A., Tavera, H., Socquet, A., 2016. Postseismic relocking of the subduction megathrust following the 2007 Pisco, Peru, earthquake. J. Geophys. Res., Solid Earth 121 (5), 3978–3995.

Savage, J.C., 1983. A dislocation model of strain accumulation and release at a subduction zone. J. Geophys. Res., Solid Earth 88 (B6), 4984–4996.

Spagnotto, S., Triep, E., Giambiagi, L., Lupari, M., 2015. Triggered seismicity in the Andean arc region via static stress variation by the Mw = 8.8, February 27, 2010, Maule Earthquake. J. South Am. Earth Sci. 63, 36–47.

Sun, T., Wang, K., Iinuma, T., Hino, R., He, J., Fujimoto, H., Kido, M., Osada, Y., Miura, S., Ohta, Y., Hu, Y., 2014. Prevalence of viscoelastic relaxation after the 2011 Tohoku-oki earthquake. Nature 514 (7520), 84.

Sun, T., Davis, E.E., Wang, K., Jiang, Y., 2017. Trench-breaching afterslip following deeper coseismic slip of the 2012 Mw 7.6 Costa Rica earthquake constrained by near-trench pressure and land-based geodetic observations. Earth Planet. Sci. Lett. 479, 263–272.

Voss, N.K., Malservisi, R., Dixon, T.H., Protti, M., 2017. Slow slip events in the early part of the earthquake cycle. J. Geophys. Res., Solid Earth 122 (8), 6773–6786.

Wang, K., Hu, Y., Bevis, M., Kendrick, E., Smalley, R., Vargas, R.B., Lauría, E., 2007. Crustal motion in the zone of the 1960 Chile earthquake: detangling earthquake-cycle deformation and forearc-sliver translation. Geochem. Geophys. Geosyst. 8 (10).

Wang, K., Hu, Y., He, J., 2012. Deformation cycles of subduction earthquakes in a viscoelastic Earth. Nature 484 (7394), 327.

Zumberge, J.F., Heflin, M.B., Jefferson, D.C., Watkins, M.M., Webb, F.H., 1997. Precise point positioning for the efficient and robust analysis of GPS data from large networks. J. Geophys. Res., Solid Earth 102 (B3), 5005–5017.